(Received 12 February 2026, Accepted 24 March 2026, Scheduled 4 May 2026)

Design and Experiment of Compact Rotary MCR-WPT Coils at MHz Band

Kunming Chen[1,2], Yanhong Li[2,*], Caiyun Dai[1], Guoqiang Liu[2], Chao Zhang[2], and Guanchen Li[2,3]

[1] College of Materials Science and Engineering, Shenyang University of Chemical Technology, China
[2] Institute of Electrical Engineering, Chinese Academy of Science, China
[3] College of Information Engineering, Shenyang Chemical University, China

ABSTRACT: Aiming to meet the contactless power supply requirements of rotary equipment, this study investigates the coil design and performance of a small resonator for magnetically coupled resonant wireless power transfer (MCR-WPT) systems operating in the MHz band. Based on the series-series (S-S) WPT circuit topology, the influence of coil inductance on the transmission characteristics of the system was analyzed. By combining the inductance calculation formula for planar spiral coils, the geometric parameters of the coil were designed with the objectives of load power $(P_{\mathrm{RL}}) > 40$ W and transmission efficiency $(\eta) > 90\%$. The rationality of the designed parameters was verified by field-circuit coupled simulation, and the influence laws of the driving frequency and transmission distance on transmission characteristics were also analyzed. The coils were wound according to the designed parameters, and both static and rotary dynamic power transfer experiments were conducted. The simulation results show that the designed coil achieves a transmission efficiency of 94.783% at a transmission distance of 50 mm in the 1 MHz, which meets the preset design objectives. The results of the static experiment and dynamic rotation experiment show that the overall operating efficiency of the system $(\eta_{\text{dc-dc}})$ is 84%. This study demonstrates the feasibility of the proposed coil design method, and the designed small coil can realize high-efficiency and stable wireless power transfer under rotary working conditions. The research findings provide a reference for the coil design and engineering application of rotary MCR-WPT systems in the MHz band and possess practical value for the contactless power supply of sensors in rotary electrical equipment operating in confined spaces.

1. INTRODUCTION

The concept of wireless power transfer was first proposed by Nikola Tesla, who successfully lit a light bulb wirelessly in his laboratory, thereby laying a solid theoretical and experimental foundation for the subsequent development of wireless power transfer technology. Following more than a century of technological iterations, various wireless power transfer technologies, including the inductively coupled type [1], microwave radiative type [2], and laser-based power transfer type [3], have matured significantly. Among them, the inductively coupled scheme has become the mainstream technology in short-range power transfer owing to its simple structure and low cost. However, this technology suffers from inherent drawbacks, such as short transmission distance, low coupling coefficient, and excessively rapid decay of transmission efficiency with distance, making it difficult to meet the demand for a contactless power supply with medium-short range and high power density [4]. In 2007, the Massachusetts Institute of Technology (MIT) took the lead in proposing magnetically-coupled resonant wireless power transfer (MCR-WPT) technology [4]. This technology overcame the distance bottleneck of traditional inductively coupled power transfer and set off a new upsurge in research on wireless power transfer technology. Based on the principle of resonance, magnetically-coupled resonant wireless power transfer realizes energy coupling and transmission in resonant cavities, enabling high-power and high-efficiency electric energy transmission over relatively long distances [5].

Against the backdrop of the intelligent and rotational upgrading of industrial equipment, underwater detection, biomedicine, intelligent transportation, and other fields, rotational wireless power transfer technology has become a key solution to the power supply challenges of rotating equipment (such as rotating shaft sensors, robot joints, autonomous underwater vehicles, rotating ultrasonic machining equipment and rotating spacecraft components). This is because of its core advantages, including the absence of physical contact, elimination of brush-slip ring wear, freedom from cable entanglement, and adaptability to dynamic rotational operating conditions [6–9]. Traditional power supply methods suffer from drawbacks such as rapid wear and aging, poor contact, susceptibility to sparking, and high maintenance costs. Additionally, battery power supply was limited by short endurance and high maintenance costs. These issues severely restrict the reliability and service life of equipment [8, 10, 11]. In contrast, rotational wireless power transfer (R-WPT) systems achieve contactless energy transfer under rotating conditions through electromagnetic coupling between coils. This technology resolves the inherent defects of contact-based power supplies while satisfying the special requirements of rotating equipment for dynamic balance and structural com-

* Corresponding author: Yanhong Li (liyanhong@mail.iee.ac.cn).

pactness [12–14]. As the core electromagnetic coupling component of R-WPT systems, the coil design directly determines the transmission efficiency, coupling stability, anti-rotational misalignment capability, and application adaptability of the system. The rationality of its structural topology, parameter matching, material selection, and optimization methods constitutes a core bottleneck restricting the development of rotational wireless power transfer technology toward high-power, miniaturized, and stable power supply [8, 14].

Currently, many scholars have conducted targeted investigations on the coil design of MCR-WPT systems and achieved numerous groundbreaking results in areas such as structural topology innovation, winding configuration optimization, intelligent parameter regulation, material selection, and application-specific adaptation. Ref. [15] revealed, through studies on various coil types and parameters, that the quality factor of a coil is positively correlated with its coil diameter and wire diameter, and negatively correlated with the turn-to-turn spacing. Ref. [16] realizes a uniform magnetic field distribution on the plane of the receiving coil by superimposing the magnetic fields generated by spiral and densely wound coils, which effectively reduces the efficiency fluctuations caused by positional misalignment. A double-layer printed circuit board (PCB) coil was designed in [17], by optimizing key parameters, such as trace width and turn-to-turn spacing, and it improved the transmission efficiency under offset conditions to 46.6%, achieving a favorable balance between manufacturing simplicity and adaptability to low-power devices. Furthermore, Ref. [18] combined machine learning with meta-heuristic algorithms to construct a neural network model for predicting coil efficiency and implemented parametric optimization of implantable biomedical coils by integrating a genetic algorithm and coyote optimization algorithm, thereby satisfying the dual design requirements of coil miniaturization (size $<$ 20 mm) and high-efficiency power transmission.

This study focuses on the wireless power supply demands of sensors in equipment containing rotating mechanisms in confined spaces. With the core objective of achieving dynamic rotational wireless power transfer using compact coils and guided by the requirement for high reliability and high efficiency in such scenarios, research on coil design and system transmission characteristics was conducted. First, the influence of coil inductance on the system transmission characteristics was analyzed through theoretical calculations, from which the reasonable range of coil parameters is determined, and the coil design was completed. Subsequently, the rationality of the coil design method adopted in this study was verified by mutual validation of the simulation and experiment. Then, the effects of the driving frequency and transmission distance on the system transmission characteristics were investigated via field-circuit coupling analysis, and the parameters were further calibrated to ensure their suitability for the intended scenario. Finally, dynamic rotation experiments were performed under the determined parameters, and the system transmission characteristics at different rotational speeds were measured to verify the feasibility and stability of the proposed scheme under practical rotational operating conditions.

2. ANALYSIS OF CIRCUIT TRANSMISSION CHARACTERISTICS

The transmission characteristics of the circuit were analyzed according to the equivalent diagram of the SS-WPT circuit, as shown in Fig. 1 [15]. In the diagram, I_1 and I_2 represent the primary-side current and secondary-side current, respectively; C_p and C_s denote the resonant capacitors on the primary and secondary sides, respectively; R_p and R_s represent the internal resistances of the primary and secondary sides, respectively; L_p and L_s are the inductances of the primary-side coil and secondary-side coil, respectively; M is the mutual inductance between the two coils; R_L represents the load resistance; and U_s is the equivalent voltage source.

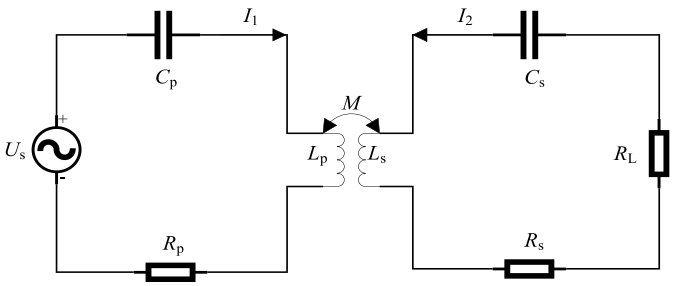

FIGURE 1. Equivalent circuit of S-S WPT system.

When the system operates steadily with a high-frequency alternating current of frequency f input from the voltage source U_s, the angular frequency $\omega = 2\pi f$. The primary loop impedance Z_1 and secondaryloop impedance Z_2 are express as follows [15]:

$$Z_1 = \mathrm{j}\omega L_p + \frac{1}{\mathrm{j}\omega C_p} + R_p \tag{1}$$

$$Z_2 = \mathrm{j}\omega L_s + \frac{1}{\mathrm{j}\omega C_s} + R_s \tag{2}$$

Based on Kirchhoff's laws, the loop voltage equation can be formulated, and the primary current I_1, input power P_{in}, load power P_{RL}, and transmission efficiency η of the system were calculated [19].

$$I_1 = \frac{(Z_2 + R_L)U_s}{(\omega M)^2 + Z_1(Z_2 + R_L)} \tag{3}$$

$$P_{\text{in}} = \frac{U_s^2 \left|Z_2 + R_L\right|^2 \mathrm{Re}\left[Z_1 + \frac{(\omega M)^2}{Z_2 + R_L}\right]}{\left|Z_1(Z_2 + R_L) + (\omega M)^2\right|^2} \tag{4}$$

$$P_{\text{RL}} = \frac{U_s^2 \left|\mathrm{j}\omega M\right|^2 R_L}{\left|Z_1(Z_2 + R_L) + (\omega M)^2\right|^2} \tag{5}$$

$$\eta = \frac{\left|\mathrm{j}\omega M\right|^2 R_L}{\left|Z_2 + R_L\right|^2 \mathrm{Re}\left[Z_1 + \frac{(\omega M)^2}{Z_2 + R_L}\right]} \tag{6}$$

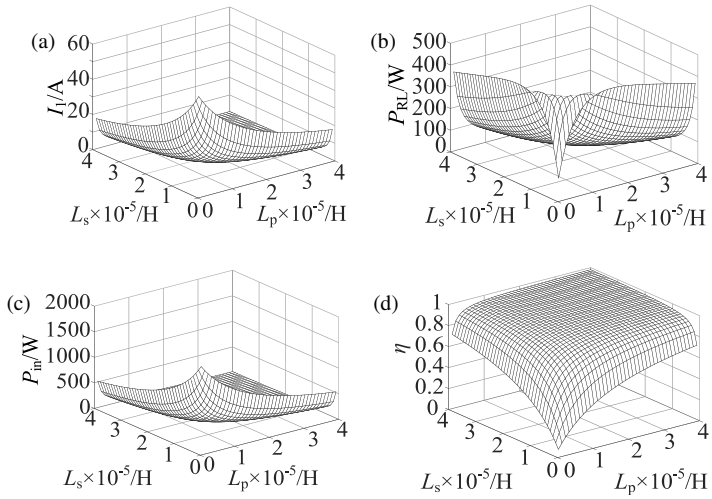

FIGURE 2. Surface plots of transmission characteristics as functions of inductance values. (a) Primary current. (b) Load power. (c) Input power. (d) Transmission efficiency.

3. SIMULATION ANALYSIS

To accurately determine the geometric parameters and transmission characteristics of the coupled coils, the variation curves of the transmission characteristics with respect to coil inductance were obtained through theoretical calculation of the circuit transmission characteristics, and the precise coil parameters were determined by selecting an appropriate inductance value. Based on the determined parameters, a finite element simulation model was established for the field-circuit coupled analysis to validate the rationality of the designed coils.

3.1. Determination of Geometric Parameters

An optimal design of the resonator was essential for achieving superior coupling performance. This section analyzes the influence of the primary and secondary coils' inductance on the system's power transfer characteristics. The designed resonator was configured with a coupling coefficient $k \approx 0.22$, a load resistance $R_L = 50\,\Omega$, the coil resistance $R_p = R_s = 0.5\,\Omega$, an excitation voltage $U_s = 30\,\text{V}$, and a resonant frequency $f = 1\,\text{MHz}$. The inductances of the primary and secondary coils were varied in the range of 0–40 μH. Three-dimensional surface plots of the primary current, load power, input power, and power transfer efficiency as functions of inductance were obtained and are presented in Fig. 2.

The system design objectives set in this study were a load power of 40 W and a transfer efficiency between the transmitting and receiving coils of no less than 90%. Meanwhile, to limit the transmitter current and protect various circuit components, the primary current I_1 was required to be less than 2 A. Accordingly, cross-sectional planes corresponding to $I_1 = 2\,\text{A}$, $P_{\text{RL}} = 40\,\text{W}$, $P_{\text{in}} \approx 44\,\text{W}$ (calculated from P_{RL}/η), and $\eta = 90\%$ were extracted from the three-dimensional surface plot (Fig. 2), yielding the curves of the power transfer characteristics versus coil inductance, as shown in Fig. 3.

Based on the preset thresholds, the cross-sections corresponding to each target parameter in Fig. 2 were selected and projected onto the plane containing L_p and L_s, yielding the subfigures in Fig. 3. In these figures, the four regions labeled A, B, C, and D correspond to the parameter intervals where the primary current $I_1 < 2\,\text{A}$, load power $P_{\text{RL}} > 40\,\text{W}$, input power $P_{\text{in}} < 44\,\text{W}$, and transmission efficiency $\eta > 90\%$, respectively. The blank regions represent the non-target intervals where $I_1 > 2\,\text{A}$, $P_{\text{RL}} < 40\,\text{W}$, $P_{\text{in}} > 44\,\text{W}$, and $\eta < 90\%$, while the boundary values correspond to the critical thresholds of the respective parameters. To design a wireless power transfer coil with high transmission efficiency, an appropriate inductance value can be selected from the intersection of regions A, B, C, and D to achieve efficient power transfer.

By analyzing the variation of transmission characteristics with coil inductance, optimal inductance parameters can be identified to construct a magnetically coupled wireless power transfer system with high load power and high transmission efficiency. Under a resonant frequency of 1 MHz, superior transmission performance can be achieved when the coil inductance is in the range of 15–40 μH, and the inductance of the receiving coil should be selected to be equal to or greater than that of the primary coil. Conversely, if the primary coil inductance is too low, a significant increase in I_1 can occur, which is detrimental to the safe operation of the primary-side circuit components. Comprehensive analysis indicates that selecting both the primary and secondary coil inductances at approximately 20 μH enables efficient power transfer with $P_{\text{RL}} > 40\,\text{W}$ and $\eta > 90\%$.

The conventional coil structure used in MCR-WPT systems is a planar spiral coil. Ref. [19] presents a theoretical formula for calculating the inductance of this type of coil.

$$L = \frac{\mu_0 N^2 (r_{\text{out}} + r_{\text{in}})}{2} \left\{ \ln\left[\frac{2.46\,(r_{\text{out}} + r_{\text{in}})}{r_{\text{out}} - r_{\text{in}}}\right] + \frac{0.2\,(r_{\text{out}} - r_{\text{in}})^2}{(r_{\text{out}} + r_{\text{in}})^2} \right\} \quad (7)$$

where μ_0 is the permeability of free space; N is the number of coil turns; r_{out} is the outer radius of the coil; and r_{in} is its inner radius.

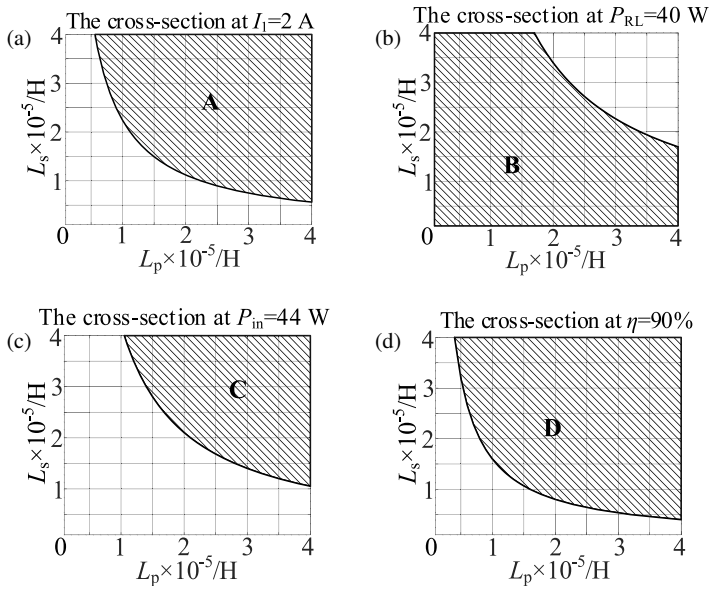

FIGURE 3. Curves of transmission characteristics versus coil inductance. (a) Primary current. (b) Load power. (c) Input power. (d) Transmission efficiency.

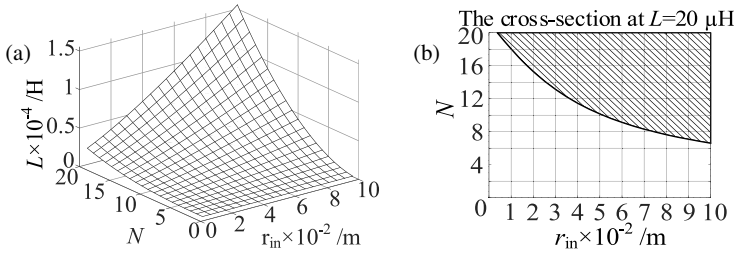

FIGURE 4. Variation of L with N and r_{in}. (a) 3D relationship of L versus N and r_{in}. (b) 2D relationship of L versus N and r_{in}.

By calculating the inductance of the spiral coil under different coil radii and numbers of turns, a three-dimensional surface plot of the inductance varying with coil radius and number of turns can be obtained. As shown in Fig. 4(a), the inductance increases with the increase in coil radius and number of turns. Therefore, to obtain a coil with an inductance of approximately 20 μH, appropriate values for the coil radius and number of turns must be determined. A cross-section corresponding to an inductance of 20 μH is extracted from the three-dimensional surface plot, as shown in Fig. 4(b), and the inductance variation region of the three-dimensional surface can be projected onto this two-dimensional cross-sectional plane.

In the cross-section shown in Fig. 4(b), the shaded region corresponds to an inductance greater than 20 μH; the white region corresponds to an inductance less than 20 μH; and the points on the curve correspond to an inductance equal to 20 μH.

The objective of this study was to implement a wireless power supply for sensors in confined spaces. Accordingly, the coil radius was minimized to the greatest possible extent. Based on this requirement, the coil parameters, namely the inner radius r_{in} and the number of turns N, were selected directly from Fig. 4(b): inner radius $r_{in} = 40$ mm, number of turns $N = 12$. Meanwhile, the transmission distance h was set to be 50 mm. This parameter combination can theoretically achieve wireless power transfer with an inductance of approximately 20 μH and a power transfer efficiency exceeding 90%.

Under high-frequency operating conditions, an appropriate increase in the number of winding turns can effectively reduce the inter-turn capacitance, thereby mitigating its adverse effects on the resonant state and stability of the system. To meet the requirements of wireless power transfer between compact coils, the turn-to-turn spacing of the coil was set to 1 mm, and the diameter of the Litz wire was 2 mm. Based on the above analysis, the final parameters of the coupled coils are summarized in Table 1.

TABLE 1. Parameters of coupling coils.

Parameters	Numerical values
Turns (N)	12
Outer radius (r_{out}/mm)	76
Inner radius (r_{in}/mm)	40
Litz wire diameter (d/mm)	2
Circle spacing (c/mm)	1
Transmission distance (h/mm)	50

TABLE 2. Simulation parameters and calculated results.

Parameters	Numerical values
Frequency (f/MHz)	1
Primary inductor (L_p/μH)	20.610
Secondary inductor (L_s/μH)	20.609
Primary resistance (R_p/Ω)	0.191
Secondary resistance (R_s/Ω)	0.194
Mutual induction (M/μH)	4.664
Coupling coefficient (k)	0.226

3.2. Field-Circuit Coupling Simulation Analysis

Based on the coil parameters obtained from the theoretical analysis, a simulation model was established, as illustrated in Fig. 5. Under the magnetic field frequency-domain simulation at 1 MHz, an excitation current of 2 A was applied to the primary coil. The coil inductance, mutual inductance, and coupling coefficient obtained from the simulation were compared with the theoretical results (listed in Table 2), validating that the proposed coil design method enabled the coil to achieve the target inductance.

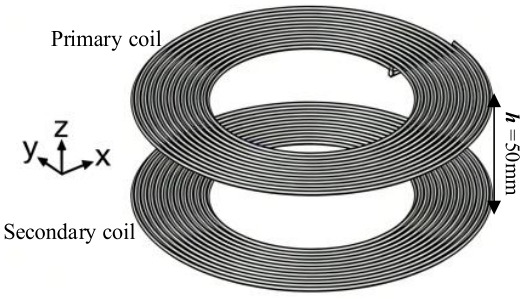

FIGURE 5. Simulation model.

The results demonstrate that the theoretically calculated inductance of the designed coil is consistent with the design specifications. The simulated values of inductance and mutual inductance are 20.610 μH (L_p), 20.609 μH (L_s), and 4.664 μH, respectively. The coupling coefficient of the coil obtained from the simulation is approximately 0.226, which is higher than the preset value and satisfies the coil design objectives.

To further verify the rationality of the coil design, the field-circuit coupled simulation was carried out. The resonant capacitor parameters in the circuit were matched according to the coil inductance obtained from the simulation. The simulated power transfer efficiency, load power, and primary-side current were calculated to be 94.719%, 48.357 W, and 1.7 A, respectively. It can be thus concluded that the selected coil parameters can achieve the desired transmission characteristics, thereby validating the correctness of the proposed coil design method from a simulation perspective.

A Class-E amplifier circuit was employed as the power supply circuit for the system. To examine the influences of the driving frequency and transmission distance on the system power transfer characteristics, a frequency-sweep simulation was performed based on the aforementioned simulation model. With a frequency step of 0.01 MHz, the driving frequency was swept over the range of 0.8–1.2 MHz, and the load power and power transfer efficiency of the theoretical circuit are computed. The results are shown in Fig. 6.

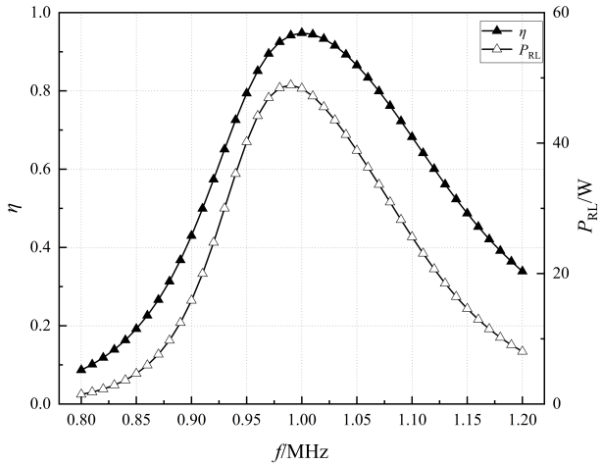

FIGURE 6. Variation of η and P_{RL} with driving frequency.

From the above calculations and simulation results, it can be seen that as the driving frequency increases, both the power transfer efficiency and load power show a trend of increasing first and then decreasing. It can be observed that transmission performances close to the maximum power transfer efficiency are attainable near the resonant frequency. Furthermore, the maximum load power of the system is achieved when the driving frequency was slightly lower than the resonant frequency.

An appropriate transmission distance enables the system to achieve excellent transmission performance. Based on the established simulation model, the transmission efficiency for different transmission distances was calculated at a resonant frequency of 1 MHz to verify whether the 50 mm transmission distance adopted in this study is reasonable. The simulation results are shown in Fig. 7.

As shown in Fig. 7, at a resonant frequency of 1 MHz, the power transfer efficiency exhibits a downward trend as the transmission distance increases. The efficiency drops below 90% when the transmission distance exceeded 65 mm. As the

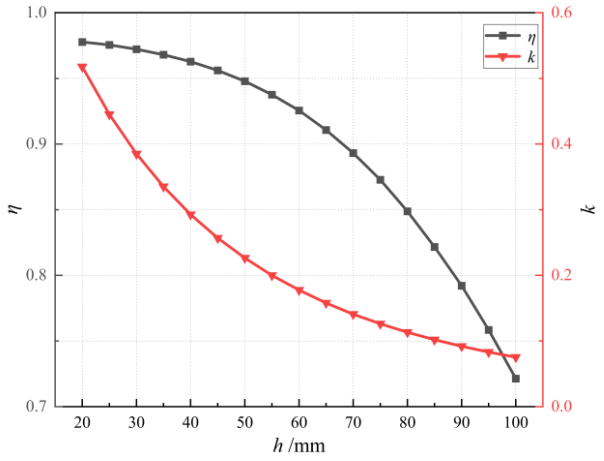

FIGURE 7. Variation of η with h at 1 MHz.

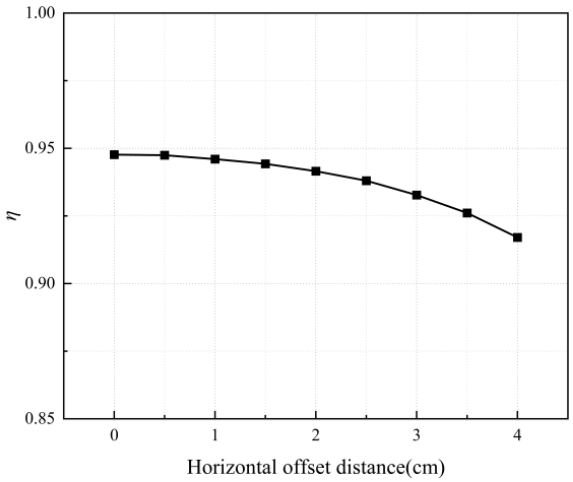

FIGURE 8. Variation of η with the horizontal offset distance.

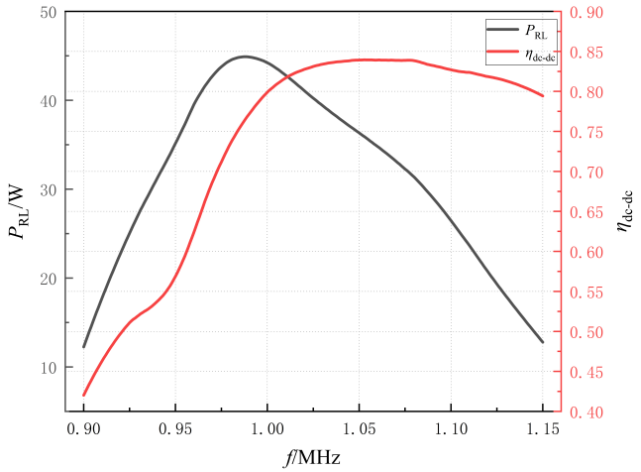

FIGURE 9. System efficiency and load power versus frequency.

transmission distance h increases, the mutual inductance between the two coils decreases, while the self-inductance of each coil remains nearly unchanged. Consequently, the coupling coefficient k decreases with increasing transmission distance, leading to a reduction in the transmission efficiency. At a transmission distance of 50 mm, as specified in the coil design of this study, the power transfer efficiency reaches 94.783%, which satisfied the experimental design objectives.

In the rotational experiment, the motor induces vibration of the experimental platform during operation, which in turn causes slight horizontal misalignment between the transmitting coil and the receiving coil. Therefore, it is necessary to perform a simulation analysis of the small-range coil offset condition, and the simulation results are shown in Fig. 8. The results indicate that the transmission efficiency, η, gradually decreases with increasing horizontal offset distance, revealing a clear negative correlation between the two variables. When the horizontal offset distance is small, the variation in η remains relatively gentle, indicating that the system has a certain tolerance to minor offsets. However, as the offset distance continues to increase, the downward trend of η becomes more pronounced, suggesting that larger horizontal offsets significantly degrade the system performance. Overall, if only a small-range coil offset occurs, its influence on transmission efficiency is minimal.

The field-circuit coupled finite element simulation results validate the feasibility of the proposed design method. This method selects appropriate inductance parameters by analyzing the influence of the coupled coil inductance on the power transfer characteristics of the system, and determines the structural parameters of the coil based on the selected inductance value.

4. EXPERIMENTAL VERIFICATION

The primary and secondary coils were wound and fabricated in accordance with the determined coil parameters to verify the feasibility of the designed coil and the accuracy of the simulation analysis. Static and dynamic power transfer experiments with the rotating receiving coil were performed separately.

4.1. Static Transmission Experiment

According to the coil parameters obtained from the simulation (Table 1), the primary and secondary coils were wound. The actual inductance values of the two coils were measured, and the corresponding resonant capacitors were selected to achieve resonance 1 MHz according to the measured inductances. The driving frequency and resonant capacitors were iteratively adjusted to bring the circuit into resonance. The measured coil inductances and the corresponding matched resonant capacitor parameters are listed in Table 3. The actual matched capacitance was smaller than the theoretical resonant capacitance, which was mainly caused by the inter-turn parasitic capacitance of the coils and measurement errors.

TABLE 3. Inductance values and matching capacitance values.

Parameters	Numerical values
Frequency (f/MHz)	1
Primary inductor (L_p/μH)	22.14
Secondary inductor (L_s/μH)	23.04
Primary resistance (R_p/Ω)	1.38
Secondary resistance (R_s/Ω)	1.47
Primary quality factor (Q_p)	100.3
Secondary quality factor (Q_s)	98.5
Mutual induction (M/μH)	4.272
Primary capacitor (C_p/pF)	1099
Secondary capacitor (C_s/pF)	1035

A 30 V DC power supply was used in the experiment. A frequency-sweep test was conducted by adjusting the driving frequency, and the load power and system efficiency at different frequencies were measured. The experimental results are shown in Fig. 9. The voltage waveforms across the switching transistor and the primary resonant capacitor (C_p) at maximum system efficiency are shown in Fig. 10.

The experimental measurements indicate that the trends of load power and system efficiency with respect to the driv-

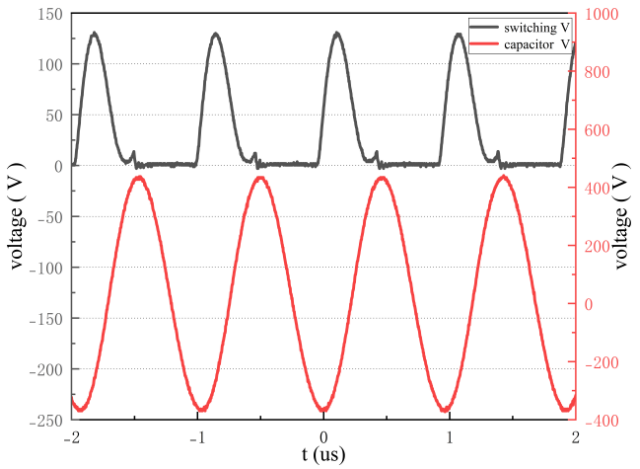

FIGURE 10. Voltage characteristics of the switching transistor and resonant capacitor.

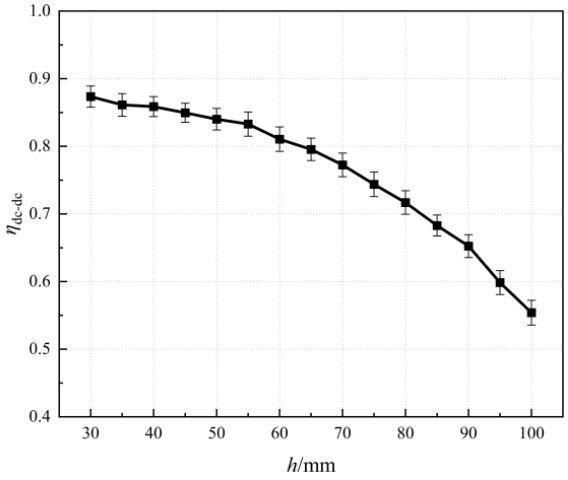

FIGURE 11. Variation trend of $\eta_{dc\text{-}dc}$ with h.

ing frequency are in good agreement with the simulation results: both initially increase and then decrease as the driving frequency increases. The maximum load power was approximately 44.9 W at a driving frequency of 0.99 MHz. When the frequency exceeded 1.03 MHz, the load power falls below 40 W and exhibits a continuous downward trend with further increases in the driving frequency. Within the frequency band of 1–1.1 MHz, the system efficiency varies slightly, reaching a maximum value of approximately 84% at a driving frequency of 1.03 MHz.

The efficiency measured in the experiment represents the overall efficiency of the system ($\eta_{dc\text{-}dc}$), rather than the transmission efficiency between the transmitting and receiving resonators. The experimental results reflect the overall system efficiency from the DC supply to the rectified load. Consequently, the experimental system incorporates several additional loss sources that are not fully account for the idealized resonator-level model: (1) switching loss and conduction loss in the Class-E inverter, (2) rectifier diode loss and filter loss on the secondary side, (3) frequency-dependent AC resistance of the Litz-wire coils under MHz operation, (4) mismatch introduced by coil parasitic capacitance and component tolerances, (5) additional wiring and measurement losses in the laboratory prototype. Furthermore, the measured inductances deviate from the design values, which shifts the actual resonant point and causes the optimum system efficiency frequency to move to 1.03 MHz rather than exactly 1 MHz. After these practical losses are considered, the gap between simulation and experiment is acceptable.

Frequency characteristic tests of the power transfer system were conducted at a transmission distance of 50 mm. The results demonstrated that when the driving frequency ranged from 1 MHz to 1.03 MHz, stable power transfer could be achieved, with a system efficiency above 80% and a load power exceeding 40 W. To verify the variation in system transmission efficiency with transmission distances, the efficiency was measured at a driving frequency of 1.03 MHz as the transmission distance varied from 30 to 100 mm. The measurement results are shown in Fig. 11.

The measured results indicate that the trend of the system transmission efficiency with respect to transmission distance is consistent with the simulation results. With other parameters kept constant, the system transmission efficiency decreases as the transmission distance increases. When the transmission distance exceeds 60 mm, the system efficiency decreased below 80%. The reduction in system efficiency is mainly attributed to the decrease in the mutual inductance between the coils as the transmission distance increases, which consequently degrades the coupling performance. This behavior can be explained by the mutual inductance equations [19]:

$$M = \frac{\mu_0 N^2 (r_{\text{out}} + r_{\text{in}})}{2} \left[\left(\frac{2}{k'} - k' \right) K(k') - \frac{2}{k'} E(k') \right] \quad (8)$$

$$k' = \sqrt{\frac{(r_{\text{out}} + r_{\text{in}})^2}{(r_{\text{out}} + r_{\text{in}})^2 + h^2}} \quad (9)$$

where μ_0 is the permeability of free space; N is the number of coil turns; $K(k')$ and $E(k')$ are the complete elliptic integrals of the first and second kinds, respectively; k' is the modulus; and h is the transmission distance between the two coils.

With all other parameters held constant, an increase in the transmission distance h directly leads to a reduction in mutual inductance. Since the self-inductance of the coils remains essentially unchanged with transmission distance, the coupling coefficient decreases accordingly, ultimately resulting in a decline in system efficiency. In addition, as shown by the simulation results of the coupling coefficient versus transmission distance in Fig. 7, the coupling coefficient exhibits a decreasing trend as the transmission distance increases, which is consistent with the above theoretical analysis. Therefore, the experimentally observed decrease in system efficiency with increasing transmission distance is jointly validated by both the theoretical analysis and the simulation results. Consequently, the coil parameters designed in this study are no longer suitable for the system operation at such a transmission distance.

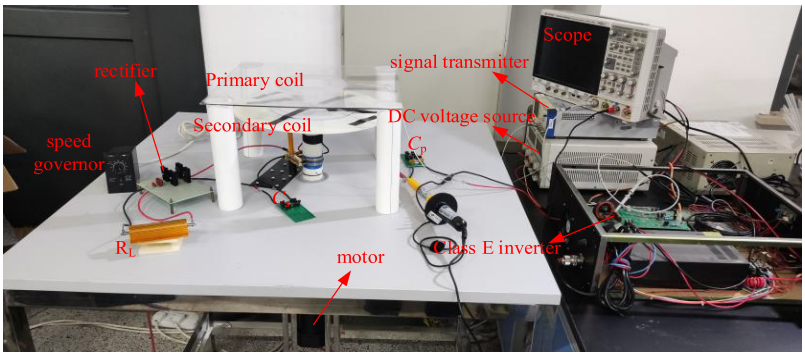

FIGURE 12. Rotary wireless power transfer system.

TABLE 4. Comparison of representative WPT coil designs reported in the literature.

Reference	[16]	[17]	[18]	This work
Coil strategy	Double-mosquito combined coil	Double-layer PCB planar spiral coil	Circular spiral coil optimized by NN + GA/COA	Compact rotary planar spiral coil
Size	Tx 300 × 300 mm; Rx 142 × 142 mm	Outer diameter: 90 mm	< 20 mm	r_{in} 40 mm; r_{out} 76 mm; 12 turns
f	85 kHz	98–100 kHz	13.56 MHz	1 MHz
Condition	50 mm; Static	Low-power system with misalignment	Inside the organism	50 mm distance; 90–450 r/min coaxial rotation
P_{out}/η	89.3 W; 83.3%	14.4 W; 83.7%	N/R; 76%	42 W; 84%
Key merit/ limitation	Strong misalignment tolerance; relatively large coil size	Easy fabrication and integration; efficiency degrades under offset	Miniaturized implant design; limited to biomedical low-power use	Compact MHz-band rotary transfer with stable dynamic performance and simple coil design

4.2. Dynamic Rotation Experiment

To realize a contactless power supply for sensors under rotational operation in confined spaces, this study investigates a wireless power transfer system with coaxially rotating receiving coil and develops a dynamic experimental platform as illustrated in Fig. 12. The coil parameters were identical to those used in the static experiments. The transmission distance was set to 50 mm and the driving frequency was set to 1.03 MHz, at which the static system achieved maximum transmission efficiency. Under these operating conditions, the effects of various rotational speeds on the system efficiency were investigated, and the measurement results are presented in Fig. 13.

Experimental measurements indicated that the WPT system can operate stably with the receiving coil during rotation. Variations in rotational speed within the range of 90–450 r/min have a negligible effect on the system efficiency and load power. The system efficiency remained stable at approximately 84% with a measurement error of approximately 1% across multiple repeated tests. The load power showed slight fluctuations with changing rotational speeds, and it was generally maintained at approximately 42 W.

5. COMPARISON WITH PREVIOUS WORKS AND DISCUSSION

To better position the proposed design with respect to prior studies, Table 4 summarizes representative WPT coil designs in terms of coil strategy, size, operating frequency, transfer condition, output power, efficiency, and key characteristics. Previous studies mainly emphasized implant miniaturization, PCB integration, or translational misalignment tolerance, whereas comparatively fewer works addressed compact rotary MCR-WPT coils operating in the MHz band.

Compared with previous studies, the proposed design is distinguished by its compact coil size, MHz-band operation, and stable power transfer under rotary conditions. Existing studies have mainly emphasized implant miniaturization, PCB integration, or tolerance to translational misalignment. In contrast, this work targets compact rotary equipment requiring a contactless power supply in confined spaces, and demonstrates stable dynamic transfer at 90–450 r/min with an efficiency of about 84% and a load power of about 42 W. Therefore, the main contribution of this work lies not only in the compact coil design itself, but also in verifying the feasibility of high-efficiency MHz-band MCR-WPT under practical rotary operating conditions.

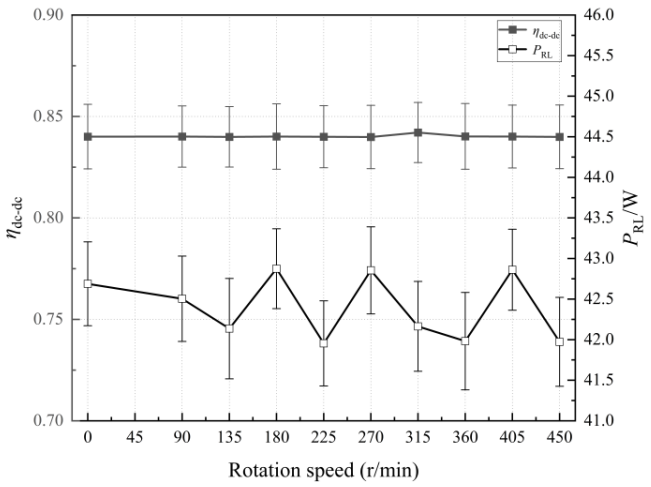

FIGURE 13. Transmission efficiency and load power of the system at different rotational speeds.

6. CONCLUSION

This study addresses the coil design of compact rotary MCR-WPT systems operating in the MHz frequency band. Based on the SSWPT circuit topology, the geometric parameters of the coupled coils are determined by analyzing the influence of coil inductance on the system transmission characteristics, combined with theoretical formulas for calculating the inductance and mutual inductance of planar spiral coils. Field-circuit co-simulations, static power transfer experiments, and dynamic rotational tests are conducted to validate the proposed coil design scheme and comprehensively evaluate the power transfer performance of the system.

The simulation results show that the inductance value of the designed coil matches the design expectation, with a coupling coefficient of 0.226. At a transmission distance of 50 mm and an operating frequency of 1 MHz, the transmission efficiency between the primary and secondary sides of the resonator reaches 94.783%, which satisfied the design target. The load power is optimized when the system driving frequency is slightly lower than the resonant frequency, and the efficiency decreased below 90% when the transmission distance exceeds 65 mm, validating the rationality of the key parameter settings. This also proves that the influence of small-scale deviations on the transmission efficiency is very small. In the static experiments, the overall system efficiency is 84% and the peak load power is 44.9 W, which are affected by practical factors such as inter-turn capacitance, inverter system losses, and rectifier circuit losses. Stable power transfer with an efficiency of over 80% and power above 40 W can be achieved within the frequency band of 1–1.03 MHz. The attenuation trend of efficiency with distance is consistent with the simulation results, and 60 mm is determined as the effective transmission distance threshold for practical applications of the proposed coil. These results demonstrate the feasibility of the proposed design scheme.

The dynamic rotational experimental results indicate that when the receiving coil rotates coaxially at speeds ranging from 90 to 450 r/min, the overall system efficiency remains stable at approximately 84%, and the load power is maintained at approximately 42 W. Stable contactless power transfer under rotational operation is achieved, which demonstrates that the proposed coil can effectively meet the dynamic power supply requirements of rotating devices.

The compact MCR-WPT coil design method based on inductance characteristic analysis proposed herein is scientifically feasible and provides clear guidelines for the coil design of MHz-band wireless power transfer systems. The derived coil parameters and power transfer characteristics offer a direct engineering reference for the contactless power supply of small rotary electrical devices such as rotating shaft sensors and robot joints. This work has practical significance for promoting the engineering application of rotary magnetically coupled resonant wireless power transfer technology and provides an experimental and theoretical foundation for subsequent research on coil structure optimization, system loss reduction, and anti-offset capability improvement.

ACKNOWLEDGEMENT

This work was supported by the National Natural Science Foundation of China (Grant numbers: 52177011 and 52577020).

REFERENCES

[1] Özüpak, Y., "Analysis and experimental verification of efficiency parameters affecting inductively coupled wireless power transfer systems," *Heliyon*, Vol. 10, No. 5, e27420, Mar. 2024.

[2] Duan, X., L. Zhou, Y. Zhou, Y. Tang, and X. Chen, "Short-distance wireless power transfer based on microwave radiation via an electromagnetic rectifying surface," *IEEE Antennas and Wireless Propagation Letters*, Vol. 19, No. 12, 2344–2348, Dec. 2020.

[3] Haga, N., J. Chakarothai, and K. Konno, "Circuit modeling of a wireless power transfer system containing ferrite shields using an extended impedance expansion method," *IEEE Transactions on Microwave Theory and Techniques*, Vol. 70, No. 5, 2872–2881, May 2022.

[4] Kurs, A., A. Karalis, R. Moffatt, J. D. Joannopoulos, P. Fisher, and M. Soljacic, "Wireless power transfer via strongly coupled magnetic resonances," *Science*, Vol. 317, No. 5834, 83–86, Jul. 2007.

[5] Wu, Y., P. Nie, Z. Wang, L. Wang, S. Hashimoto, and T. Kawaguchi, "A comprehensive review of magnetic coupling mechanisms, compensation networks, and control strategies for electric vehicle wireless power transfer systems," *Processes*, Vol. 14, No. 2, 287, Jan. 2026.

[6] Luo, H., X. Tan, K. Liu, Z. Wei, M. Cheng, and Z. Zhou, "Design of compact magnetic coupler and high-reliability transmission circuit for rotational wireless power transfer system," *Electrical Engineering*, Vol. 107, No. 9, 11 611–11 621, Apr. 2025.

[7] Guo, Y., C. Wang, and Z. Li, "FPC receiving coil for wireless power transmission to rotational axis sensors," *Journal of Power Electronics*, Vol. 25, No. 1, 160–170, 2025.

[8] Guo, Z., J. Li, L. Wang, Y. Peng, Q. Si, and G. Luo, "Self-decoupled coupler based dual-coupled LCC-LCC rotating wireless power transfer system with enhanced output power," *Journal of Power Electronics*, Vol. 25, No. 3, 416–427, 2025.

[9] Xia, K., B. Zhu, Y. Lou, and D. Huang, "A rotary wireless power transfer system with rail-type coupling structure," *IEEE Access*, Vol. 12, 63 967–63 975, Apr. 2024.

[10] Ameye, A., A. Morel, R. Recoquillé, N. Garraud, P. Gasnier, and A. Badel, "Demonstration of multiple orbit jumps in nonlinear dual-mode electrodynamic receiver for wireless power transfer," *Energy Conversion and Management: X*, Vol. 29, 101553, Jan. 2026.

[11] Danuor, P., M.-J. Oh, J.-I. Moon, and Y.-B. Jung, "Experimental verification of coil rotation and phase-shift control for enhancing wireless power-transfer efficiency," *ETRI Journal*, Vol. 47, No. 6, 1139–1151, Dec. 2025.

[12] Wang, Q., D. Wang, and J. Zhang, "A novel rotating wireless power transfer system for slipring with redundancy enhancement characteristics," *Sustainability*, Vol. 16, No. 13, 5628, Jun. 2024.

[13] Ishida, H., Y. Akatsu, T. Kyoden, and H. Furukawa, "System for wireless power transfer to rotating objects with stable power transmission based on parity-time symmetry," *Electrical Engineering*, Vol. 107, No. 1, 841–852, 2025.

[14] Tang, H., Z. Shen, R. Xie, W. Pan, X. Chen, Z. Li, and Y. Zhang, "A novel arc-shaped magnetic coupler with dual-channel receiver for rotational misalignment tolerance in AUV underwater wireless power transfer systems," *International Journal of Circuit Theory and Applications*, Vol. 53, No. 4, 1866–1878, Apr. 2025.

[15] Zhu, J., Q. Gao, Q. Liu, W. Fan, and J.-Y. Pan, "Design and parameter optimization on coupling coil in wireless power transfer system via magnetic resonance," *Advanced Technology of Electrical Engineering and Energy*, Vol. 38, No. 7, 67–72, 2019.

[16] Huang, W., J. Huang, Y. Hu, Y. Zhu, and Y. Chang, "Design and parameter optimization of double-mosquito combination coils for enhanced anti-misalignment capability in inductive wireless power transfer systems," *Electronics*, Vol. 13, No. 5, 838, Feb. 2024.

[17] Fu, Y., Y. Zhu, D. Jiang, B. Ji, and Z. Peng, "Improved design of PCB coil for magnetically coupled wireless power transfer," *Electronics*, Vol. 13, No. 2, 426, Jan. 2024.

[18] Bennia, F., A. Boudouda, and F. Nafa, "Optimal design of wireless power transfer coils for biomedical implants using machine learning and meta-heuristic algorithms," *Electrical Engineering*, Vol. 106, No. 5, 5869–5884, Mar. 2024.

[19] An, H., G. Liu, Y. Li, J. Song, and C. Zhang, "Resonator design of wireless power transfer system with broadband magnetic coupling property," *Transactions of Beijing Institute of Technology*, Vol. 39, No. 10, 1069–1074, 1080, 2019.